THE JOURNAL OF PHYSICAL CHEMISTRY C

Article

Cite This: J. Phys. Chem. C 2018, 122, 17001−17007

pubs.acs.org/JPCC

Layer-by-Layer Oxidation Induced Electronic Properties in Transition-Metal Dichalcogenides

Soumya Ranjan Das,[†] Katsunori Wakabayashi,[‡,§] Mahito Yamamoto,[§,∥] Kazuhito Tsukagoshi,[§] and Sudipta Dutta*,[†]

[†]Department of Physics, Indian Institute of Science Education and Research (IISER) Tirupati, Tirupati 517507, Andhra Pradesh, India

[‡]Department of Nanotechnology for Sustainable Energy, School of Science and Technology, Kwansei Gakuin University, Gakuen 2-1, Sanda 669-1337, Japan

[§]WPI Centre for Materials Nanoarchitechtonics (WPI-MANA), National Institute for Materials Science (NIMS), Tsukuba 305-0044, Japan

Supporting Information

Downloaded via IISER TIRUPATI on January 27, 2021 at 17:17:12 (UTC).
See https://pubs.acs.org/sharingguidelines for options on how to legitimately share published articles.

ABSTRACT: Recent progress in transition-metal dichalcogenides has opened up new possibilities for atomically thin nanomaterial based electronic device applications. Here we investigate atomic-scale self-assembled heterojunction modulated by layer-by-layer controlled oxidation in monolayer and few-layer dichalcogenide systems and their electronic properties within a first-principles framework. Pristine dichalcogenide systems exhibit semiconducting behavior. We observe reduction of the band gap for partial oxidation of the top layer. However, complete oxidation of the top layer makes the system metallic, owing to the charge transfer from the pristine to the oxidized layer, as observed in recent experiments. When the bottom layer gets partially oxidized with fully oxidized top layers, the system shows unprecedented semimetallic behavior. The appearance of valence band maximum and conduction band minimum at different k-points can introduce valley polarization. Therefore, our study shows controlled oxidation induced varying electronic properties in dichalcogenide based heterojunctions that can be exploited for advanced electronic, optoelectronic, and valleytronic device applications.

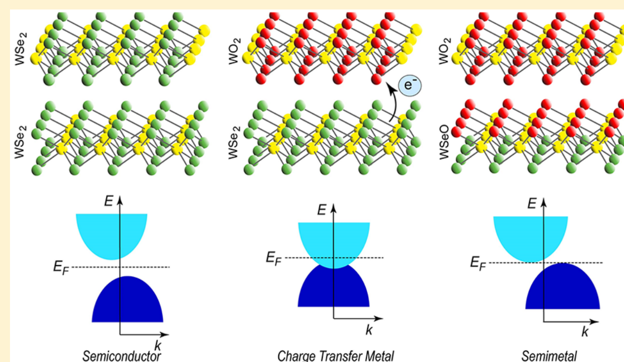

■ INTRODUCTION

Isolation of graphene has revolutionized the research of atomically thin layered materials and provided an ideal platform to consolidate the exotic properties in strictly two dimensions.[1−4] However, one major drawback of graphene is its lack of band gap, which restricts the semiconductor application of this otherwise amazing material. This fact motivated the exploration of other two-dimensional materials with varying functionalities.[5−12] Transition-metal dichalcogenides (TMDs) seem to be an ideal material in this conquest. This class of material not only shows semiconducting behavior, but also possesses high charge carrier mobility and dielectric and interesting optical properties with high mechanical strength, which can be exploited for flexible device applications.[13−19]

Although the bulk TMDs have been known for decades, the recent isolation of single or few-layer systems with controlled doping has provided precise control over the band gap.[20−30] This opens up new horizons for cutting edge device applications in field-effect transistors,[31−34] photodetectors, and diodes.[35−40] Owing to the absence of any dangling bonds on the surface of pristine layered dichalcogenides, they are mostly chemically passive. However, the edges or any defect sites are vulnerable to chemical reactivity.[41] Our recent joint experimental and theoretical study on oxidation of layered WSe_2 material in ozone environment shows that the Se atoms along the edges are preferentially replaced by O atoms.[42] However, the oxidation of the top layer at a certain temperature creates an amorphous oxide composite that protects the underlying layers from further oxidation. The oxidation of the next layer is only possible at elevated temperature. This procedure clearly shows the temperature regulated layer-by-layer oxidation of WSe_2.[42]

Further study shows that the underlying WSe_2 layer gets hole-doped by surface charge transfer to the top oxidized layer, resulting in large on-current and hole mobility.[43] This procedure of doping the TMDs has been shown to be more advantageous for field-effect transistor applications due to enhanced control on doping, as compared to the previous

Received: June 19, 2018
Published: July 2, 2018

 © 2018 American Chemical Society

proposals based on p-type Ohmic contacts[44−47] or low resistance electrochemically doped graphene contacts.[48] In this paper, we investigate the gradual layer-by-layer oxidation of layered TMDs, e.g., WSe_2 and MoS_2, systematically and its impact on the electronic properties within *ab initio* calculations. We present the results of the WSe_2 system in the paper and choose to provide the results of the MoS_2 system in the Supporting Information with reference in the main text, wherever necessary.

■ COMPUTATIONAL DETAILS

For structural relaxation and for electronic property investigation, we adopt the first-principles calculations as implemented in SIESTA.[49] We perform the calculations within generalized gradient approximation (GGA) with Perdew−Burke−Ernzerhof (PBE) exchange and correlation functional.[50] Spin polarized calculations have been performed with an antiferromagnetic spin orientation guess for the initial wave function. The double-ζ polarized (DZP) basis set has been considered with energy cutoff of 400 Ry for the real space mesh size. All the structures have been relaxed along with the relaxation of lattice constants until the force on each atom reaches 0.04 eV/Å and sufficient vacuum has been created along the nonperiodic direction (z-direction in present case) to avoid any interactions within adjacent unit cells. We consider Brillouin zone sampling over a 20 × 20 × 1 Monkhorst−Pack grid for two-dimensional structures. Note that the pseudopotentials of the atoms have been generated within a Troullier−Martins scheme with nonrelativistic electrons.

■ RESULTS AND DISCUSSION

In Figure 1a, we show the schematic picture of trilayer WSe_2, where the top layer is "fully oxidized", the middle layer is "partially oxidized" with upper surface Se atoms replaced by O atoms, and the bottom layer is "pristine WSe_2". Although during the experiment the oxidation seems to result in an amorphous WO_x ($x < 3$) structure,[42] we maintain the crystallinity for simplicity in computation. As can be seen, the 2H-WSe_2 layers represent a trigonal prismatic geometry. Note that we replace only the Se atoms by O atoms, keeping the W atoms intact, since it is energetically more favorable.[42] The hexagonal Brillouin zone arising from the honeycomb lattice is shown Figure 1b.

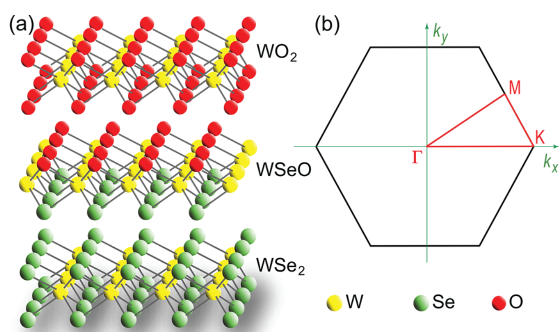

Figure 1. (a) Schematic representation of partially oxidized trilayer 2H-WSe_2 with trigonal prismatic structure. In the top layer, all the Se atoms are replaced by O atoms to make it a WO_2 layer. In the middle layer, the Se atoms of the top surface are replaced by O atoms to make it WSeO stoichiometry. The bottom layer remains intact as WSe_2. (b) The hexagonal Brillouin zone of WSe_2 with location of high-symmetric points.

To start with, we consider the experimental crystal structure of bulk WSe_2 and pick up its two-dimensional mono-, bi-, tri-, and tetralayer counterparts. Then we optimize their geometries before and after replacing the Se atoms by O atoms one-by-one from the top to the bottom layers, as illustrated in Figure 2a, and calculate their stability. As can be seen from Figure 2b, the replacement of Se atoms by O atoms leads to higher stabilization. The stabilization energy is defined as $E_{stabilization} = E_{total} - \sum_i N_i E_i$. Here, E_{total} is the total energy of the system. N_i and E_i are the number of ith species and energy of a single atom of ith species, respectively. Note that the stabilization energies in Figure 2b are scaled with respect to the number of layers. As can be seen, the stabilization energies of the systems before oxidation, i.e., for WSe_2 stoichiometry, and stabilization energies after full oxidation, i.e., for WO_2 stoichiometry, are almost independent of the number of layers with slightly higher stabilization for the increased number of layers, due to small interlayer interactions. Figure 2b shows that, after each successive oxidation, the systems gain higher stability, indicating stable structures of both partially or fully oxidized systems. Moreover, the increase in the number of O replacements increases the slope of the stabilization energy, indicating the fact that the oxidized systems are more prone for further oxidation, probably subjected to elevated temperature.

However, the temperature controlled layer-by-layer oxidation cannot be accounted for in the present calculations because we have calculated the ground state energies of all the systems at zero temperature. Moreover, each oxidation step is associated with the activation energy that needs to be overcome by elevating the reaction temperature and that can be tracked by investigating the transition states. These calculations are out of scope of the present study. Here we want to show that, by controlling the oxidation level, one can regulate a broad spectrum of electronic properties in layered TMDs, which can be useful for designing advanced electronic devices.

Note that, within the experimental environment, the top oxidized layer seems to form an amorphous composite, losing its crystallinity, as inferred from Raman spectroscopy measurements.[42,43] Our structural analysis reveals that the W−O bond length is considerably lower than the W−Se bond length (see Figure S1), introducing strain to the total structure. Therefore, the thermal agitation at higher temperature is expected to make the oxidized WSe_2 layers amorphous as the oxidation progresses. Due to the presence of this amorphous composite, the ozone cannot reach the underlying layer. Only at elevated temperature does the higher diffusion due to enhanced kinetic energy help the ozone to reach the underlying layers, and the subsequent oxidation takes place. This scenario explains the layer-by-layer oxidation of WSe_2. However, we are hopeful that, with increasing experimental sophistication, it will be possible to minimize the effect of thermal agitation to produce partially and fully oxidized crystalline TMD layers. Nevertheless, we have performed phonon dispersion calculations for a monolayer of pristine, partially oxidized, and fully oxidized systems and found all the structures to be stable (see Figure S2).

Furthermore, we explore the effect of oxidation over the electronic properties. We have investigated the electronic properties of oxidized layered WSe_2 systems and compare

DOI: 10.1021/acs.jpcc.8b05857
J. Phys. Chem. C 2018, 122, 17001−17007

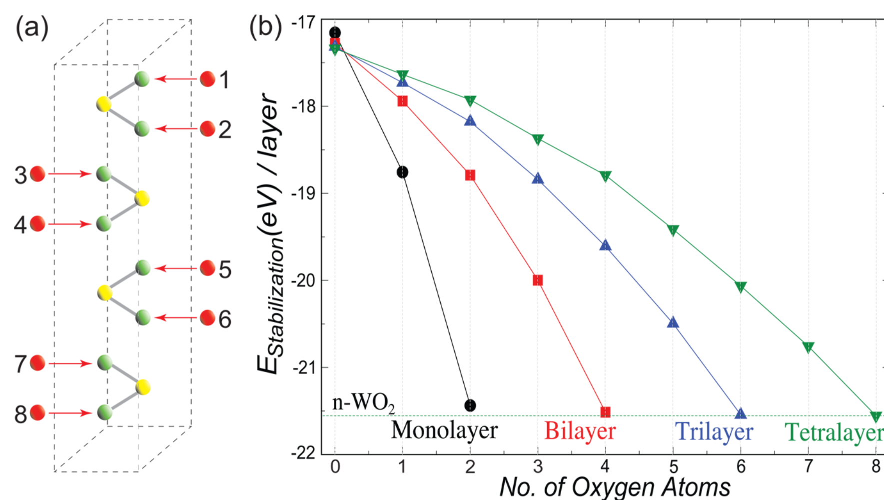

Figure 2. (a) Tetralayer WSe_2 unit cell is shown in the dashed box. The numeric values associated with the O atoms show the gradual order of replacements of Se atoms by O atoms. (b) Stabilization energies per layer of the mono-, bi-, tri-, and tetralayer WSe_2 systems as a function of the gradual increase in O atoms by replacment of the Se atoms, as shown in part a. The horizontal line indicates the stabilization energy per layer for the fully oxidized WO_2 systems.

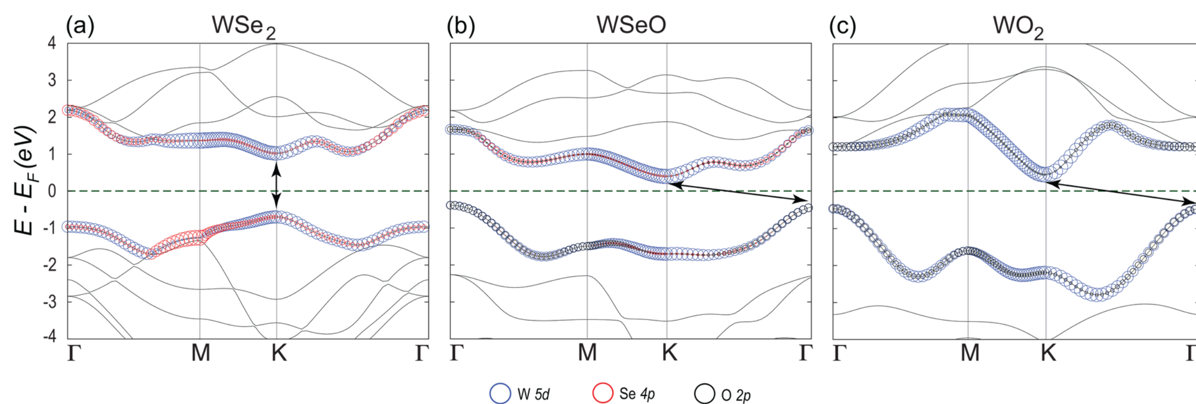

Figure 3. Band structures of monolayer (a) WSe_2, (b) WSeO (with replacement of Se atoms by O atoms in only one surface), and (c) WO_2 (with complete replacement of all Se atoms by O atoms). The horizontal dashed (vertical) lines show the location of Fermi energy (high-symmetric points). The arrows show the (a) direct or (b, c) indirect band gaps. The blue, red, and black circles show the contributions from the 5d orbital of W, 4p orbital of Se, and 2p orbital of O, respectively, for the top of the valence band and bottom of the conduction band. The size of the circles is directly proportional to the amount of contribution.

these with those of pristine WSe_2. We have considered all oxidized systems as depicted in Figure 2a along with the fully oxidized layered WO_2 system. It is known that only the monolayer of transition-metal dichalcogenides is a direct band gap semiconductor.[51−53] The top of the valence bands and the bottom of the conduction bands originate from 5d orbitals of W and 4p orbitals of Se, as can be seen from the wave function contribution in the fat-band plot in Figure 3a. Note that the larger the size of the circles is, the higher the orbital contributions are in the fat-band plots.

Replacement of the Se atom from one surface of the monolayer WSe_2 reduces the gap and makes the gap indirect, as can be seen in Figure 3b. Now the top of the valence bands originates from the 5d orbitals of W and 2p orbitals of the O. This makes the dispersion of the top of the valence bands in the WSeO system distinct as compared to that of the pristine monolayer. In this case, the valence band maximum appears at the Γ point. The bottom of the conduction band, however, still has a major contribution from the 5d orbitals of W and 4p orbitals of Se, with almost identical dispersion behavior as observed in pristine monolayer WSe_2. As a result, the band gap becomes indirect. The reduction of the band gap in a partially oxidized system, WSeO, is due to the intralayer charge transfer from the 5d orbitals of W to the 2p orbitals of O, as can be seen from Table S1. The charge transfer happens because of higher electronegativity of O as compared to Se. Since more localized d-electrons move to the p orbitals, their mobility increases, causing the reduction in band gap. After full oxidation to WO_2, the band gap remains semiconducting and indirect, with both the top of valence bands and bottom of conduction bands originating from the 5d orbital of W and the 2p orbital of O (see Figure 3c). Note that here the dispersions of these two bands are completely different than in the previous two cases. Due to this direct to indirect band gap transition upon oxidation, the peak in photoluminescence disappears,[42] and this property can be exploited for photodetector applications. All these observations are consistent for monolayer MoS_2 and its oxidized counterparts also (see Figure S3). These observations indicate the distinct nature of oxygen as compared to the other members of the chalcogen family.

An increase in the number of layers of TMDs beyond the monolayer, including the bulk TMDs, is known to result in

DOI: 10.1021/acs.jpcc.8b05857
J. Phys. Chem. C 2018, 122, 17001−17007

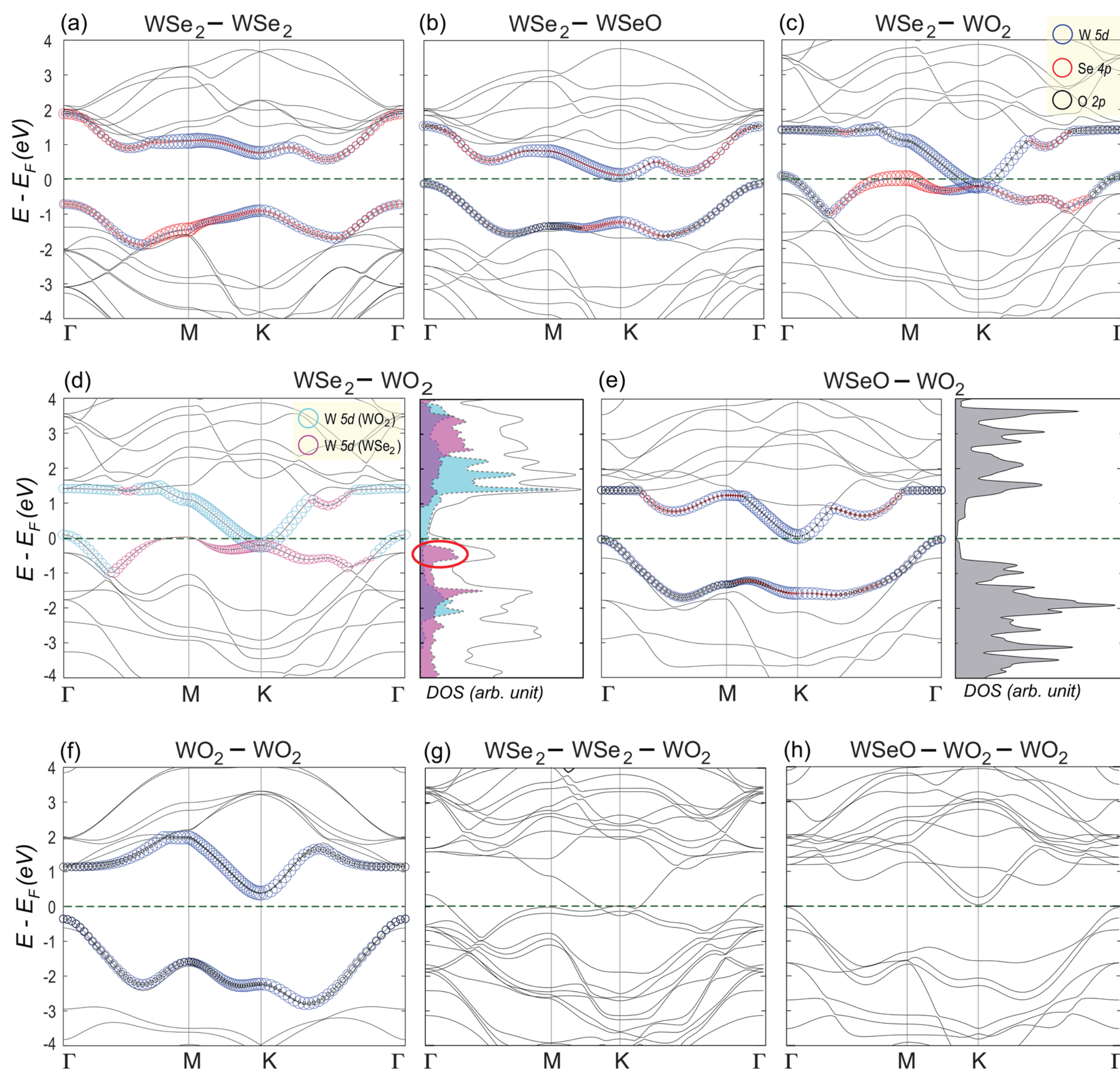

Figure 4. Band structures of bilayer (a) WSe_2–WSe_2, (b) WSe_2–WSeO, (c) WSe_2–WO_2, (d) WSe_2–WO_2 (along with fat-band plot for 5d orbital of W atoms in WO_2 (cyan) and WSe_2 (magenta) layer and their projected DOS), (e) WSeO–WO_2 (along with the DOS plot), and (f) WO_2–WO_2 systems. The blue, red, and black circles show the contributions from the 5d orbital of W, 4p orbital of Se, and 2p orbital of O, respectively, for the top of the valence bands and bottom of the conduction bands. The size of the circles is directly proportional to the amount of the contribution. Note that the purple color region in the projected DOS plot in part d arises from the overlap of cyan and magenta colors, indicating a contribution from the 5d orbital of W atoms in both WO_2 and WSe_2 layers. Parts g and h show the band structure of trilayer oxidized systems, WSe_2–WSe_2–WO_2 and WSeO–WO_2–WO_2, respectively. The horizontal dashed (vertical) lines show the location of the Fermi energy (high-symmetric points).

indirect band gap semiconductors.[51,52] The bilayer pristine WSe_2 shows an indirect band gap, as expected (see Figure 4a). The top of the valence bands and the bottom of the conduction bands originate from the 5d orbital of W and 4p orbitals of Se atoms. However, unlike the pristine monolayer system, the valence band maximum moves to the Γ point, whereas the conduction band minimum moves from the K point toward the Γ point.

The replacement of the Se atom at the top surface of the top layer reduces the indirect band gap, and the conduction band minimum shifts back to the K point (see Figure 4b). Similar to the monolayer WSeO system, here also the top of the valence bands are made of 5d orbitals of W and 2p orbitals of O, resulting in distinct dispersion as compared to the pristine system. The band gap reduction can be attributed to the intralayer charge transfer from 5d orbitals of W to 2p orbitals of O (see Table S1), making the electrons more mobile. Note that there is no interlayer charge transfer within the bottom WSe_2 and top WSeO layers.

When the top layer becomes fully oxidized to WO_2, the conduction band crosses the Fermi energy, and band mixing between the valence and conduction band takes place at the K point (see Figure 4c). Moreover, the top of the valence bands also crosses the Fermi energy at the Γ point. As a result, the system shows metallic behavior, which agrees with the experimental observation.[43] Note that both single layer WSe_2 and WO_2 are semiconducting. However, when they are stacked over each other, they exhibit metallic behavior. Our charge density analysis shows interlayer charge transfer from the WSe_2 to the WO_2 layer (Table S1), owing to higher electronegativity of O as compared to Se, and consequent higher electronegativity of the WO_2 layer. Therefore, the bottom WSe_2 layer

DOI: 10.1021/acs.jpcc.8b05857
J. Phys. Chem. C 2018, 122, 17001−17007

is expected to become hole-doped and show p-type conduction, as observed in experiment.[43] Notice that the conducting behavior is appearing from the 5d orbital of W and 2p orbital of O atoms. Although a band originating from the 4p orbitals of Se atoms appears at the Fermi energy near the M point, its dispersion-less character indicates localized electrons. Now the question is the following: Does the metallic behavior appear from the 5d orbitals of W in the fully oxidized WO_2 layer or in the underlying WSe_2 layer? For that, we have calculated the wave function contribution from W atoms in each layer and their projected density of states (DOS) and presented them in Figure 4d. As can be seen, the nonzero DOS at Fermi energy is appearing from the 5d orbitals of W atoms in the fully oxidized WO_2 layer. This does not explain the experimental observation of p-type conduction in the WSe_2 layer. This can be attributed to underestimation of interlayer charge transfer in our calculation with the crystalline WO_2 layer. In an experimental environment, the formation of amorphous WO_x ($2 < x < 3$) is expected to pull more electrons from the underlying WSe_2, causing higher hole doping due to its enhanced electronegativity. As a result, the Fermi energy shifts downward and aligns with the top of the valence bands, that actually originates from the 5d orbitals of W in pristine WSe_2 layer. The large projected DOS from these orbitals, as can be seen from the encircled region in the DOS plot along with the vanishing projected DOS from W atoms in WO_2 layer, ensures p-type conduction in the pristine WSe_2 layer. The metallic behavior might restrict its device application. However, exposure to air can be a viable way to regulate the charge transfer and consequent doping concentration to tune the electronic properties, as proposed in recent experimental studies.[43,53−58]

Further oxidation of the bottom layer results in a stacked partially oxidized WSeO and fully oxidized WO_2 bilayer system. Surprisingly, this system does not show any interlayer charge transfer and no band crossing at the Fermi energy. On the contrary, it shows zero band gap but zero density of states at Fermi energy (see Figure 4e), indicating semimetallic behavior. However, unlike graphene, the valence band maximum (at Γ point) and the conduction band minimum (at K point) appear at different k-points. This results in an unprecedented semimetallic property, which requires electron−electron or electron−phonon coupling to excite the electrons from valence to conduction band through inter-k scattering. This unique behavior provides a new platform for tuning the electron transport and the on−off current in electronic devices based on TMDs. Moreover, since the valence band maximum and conduction band minimum are well-separated in *k*-space, it is expected to show valley polarization and can be exploited for valleytronics applications.[18,59] This exotic behavior exists in neither monolayer WSeO nor WO_2 and therefore can be considered as a new topological phase of charge carriers originating at the interface. Note that similar Γ−K valley polarization has recently been observed in trilayer hole-doped WSe_2.[60]

After complete oxidation to bilayer WO_2, the system becomes an indirect band gap semiconductor (see Figure 4f) as its monolayer counterpart. The appearance of nearly degenerate bands from both the layers indicates very small interlayer interactions.

Our further investigations of trilayer WSe_2 with gradual oxidation result in similar observations. Whenever one layer becomes fully oxidized to WO_2, it attracts the electrons from the underlying WSe_2 layer making it hole-doped (see Table S1), and subsequently, the system shows metallic behavior (see Figure 4g). Note that here the valence band maximum at the K point, which originates from 5d orbitals of W in the WSe_2 layer, appears at the Fermi energy. Hence, the p-type conduction through pristine WSe_2 layers can be observed in our calculation. Higher hole doping in the experimental environment shifts the Fermi energy further down to show a higher p-type current through WSe_2 layers. In case of the bottom WSeO layer with stacked WO_2 layers on it, we observe semimetallic behavior (see Figure 4h) without any net interlayer charge transfer. All of these observations are consistent with oxidized layered MoS_2 systems as well (see Figures S4 and S5 and Table S2). This indicates that these behaviors appear to be universal in the case of TMDs.

■ CONCLUSIONS

In conclusion, we have investigated the stepwise layer-by-layer oxidation of monolayer to few-layer TMD systems, WSe_2 and MoS_2, along with their electronic properties within *ab initio* calculations. We observe that the oxidation of monolayer WSe_2 transforms the direct band gap semiconductor into an indirect band gap semiconductor with a reduced band gap. The reduction of the band gap is attributed to the change of energy dispersion and intralayer charge transfer from the 5d orbital of W to the 2p orbital of O. Although the multilayer TMDs exhibit indirect band gap semiconducting properties, full oxidation of the top layer into WO_2 induces metallic behavior. This happens due to interlayer electron transfer from an underlying pristine layer to the top oxidized layer, making the pristine layer hole-doped. As a result, the system is expected to show p-type charge conduction. Our results are in complete agreement with recent experimental findings.[43] When the bottom layer is partially oxidized having stoichiometric WSeO with fully oxidized WO_2 layers on top of it, the system exhibits semimetallic behavior. Electron conduction in this system is possible only by introducing inter-k scattering in terms of electron−electron or electron−phonon coupling. This topological phase of interface charge carriers with valley polarization will tempt further theoretical explorations. Moreover, this unprecedented property provides a unique way of tuning electronic properties in TMDs that can be exploited for advanced electronic and optoelectronic device applications.

■ ASSOCIATED CONTENT

Supporting Information

The Supporting Information is available free of charge on the ACS Publications website at DOI: 10.1021/acs.jpcc.8b05857.

Average W−Se and W−O bond lengths in pristine and oxidized layered systems; phonon spectrum of monolayers of WSe_2, WSeO, and WO_2; band structure of mono-, bi-, and trilayer MoS_2 and its oxidized counterparts; band structure of trilayer WSe_2 and its oxidized counterparts; and tables of charge densities on each atom in mono-, bi-, and trilayer pristine and oxidized WSe_2 and MoS_2 (PDF)

■ AUTHOR INFORMATION

Corresponding Author

*E-mail: sdutta@iisertirupati.ac.in.

ORCID

Sudipta Dutta: 0000-0002-8944-813X

DOI: 10.1021/acs.jpcc.8b05857
J. Phys. Chem. C 2018, 122, 17001−17007

Present Address

‖Institute of Scientific and Industrial Research, Osaka University, Ibaraki, Osaka 567-0047, Japan.

Notes

The authors declare no competing financial interest.

■ ACKNOWLEDGMENTS

S.R.D. and S.D. thank IISER Tirupati for Intramural Funding and Science and the Engineering Research Board (SERB), Department of Science and Technology (DST), Government of India, for the Early Career Research Award grant (ECR/2016/000283). K.W. acknowledges support from JSPS KAKENHI Grants JP25107005, JP15K21722, and JP15K13507. S.D. and K.W. acknowledge the financial support from Hyogo Overseas Research Network (HORN). S.D. and K.W. acknowledge the financial support for international collaboration of Kwansei Gakuin University.

■ REFERENCES

(1) Geim, A. K.; Novoselov, K. S. The Rise of Graphene. *Nat. Mater.* **2007**, *6*, 183−191.

(2) Castro Neto, A. H.; Guinea, F.; Peres, N. M. R.; Novoselov, K. S.; Geim, A. K. The Electronic Properties of Graphene. *Rev. Mod. Phys.* **2009**, *81*, 109−162.

(3) Wakabayashi, K.; Dutta, S. Nanoscale and Edge Effect on Electronic Properties of Graphene. *Solid State Commun.* **2012**, *152*, 1420−1430.

(4) Allen, M. J.; Tung, V. C.; Kaner, R. B. Honeycomb Carbon: A Review of Graphene. *Chem. Rev.* **2010**, *110*, 132−145.

(5) Novoselov, K. S.; Mishchenko, A.; Carvalho, A.; Castro Neto, A. H. 2D Materials and Van der Waals Heterostructure. *Science* **2016**, *353*, aac9439.

(6) Jariwala, D.; Marks, T. J.; Hersam, M. C. Mixed Dimensional Van der Waals Heterostructures. *Nat. Mater.* **2017**, *16*, 170−181.

(7) Gunjakar, J. L.; Kim, I. Y.; Lee, J. M.; Jo, Y. K.; Hwang, S.-J. Exploration of Nanostructured Functional Materials Based on Hybridization of Inorganic 2D Nanosheets. *J. Phys. Chem. C* **2014**, *118*, 3847−3863.

(8) Bhimanapati, G. R.; Lin, Z.; Meunier, V.; Jung, Y.; Cha, J.; Das, S.; Xiao, D.; Son, Y.; Strano, M. S.; Cooper, V. R.; et al. Recent Advances in Two-Dimensional Materials Beyond Graphene. *ACS Nano* **2015**, *9*, 11509−11539.

(9) Das, S.; Robinson, J. A.; Dubey, M.; Terrones, H.; Terrones, M. Beyond Graphene: Progress in Novel Two-Dimensional Materials and Van der Waals Solids. *Annu. Rev. Mater. Res.* **2015**, *45*, 1−27.

(10) Akinwande, D.; Petrone, N.; Hone, J. Two-Dimensional Flexible Nanoelectronics. *Nat. Commun.* **2014**, *5*, 5678.

(11) Kong, X.; Liu, Q.; Zhang, C.; Peng, Z.; Chen, Q. Elemental Two-Dimensional Nanosheets Beyond Graphene. *Chem. Soc. Rev.* **2017**, *46*, 2127−2157.

(12) Li, S.-L.; Tsukagoshi, K.; Orgiu, E.; Samori, P. Charge Transport and Mobility Engineering in Two-Dimensional Transition Metal Chalcogenide Semiconductors. *Chem. Soc. Rev.* **2016**, *45*, 118−151.

(13) Wang, Q. H.; Kalantar-Zadeh, K.; Kis, A.; Coleman, J. N.; Strano, M. S. Electronics and Optoelectronics of Two-Dimensional Transition Metal Dichalcogenides. *Nat. Nanotechnol.* **2012**, *7*, 699−712.

(14) Chhowalla, M.; Shin, H. S.; Eda, G.; Li, L.-J.; Loh, K. P.; Zhang, H. The Chemistry of Two-Dimensional Layered Transition Metal Dichalcogenide Nanosheets. *Nat. Chem.* **2013**, *5*, 263−275.

(15) Casademont, H.; Fillaud, L.; Lefevre, X.; Jousselme, B.; Derycke, V. Electrografted Fluorinated Organic Ultrathin Film as Efficient Gate Dielectric in MoS_2 Transistors. *J. Phys. Chem. C* **2016**, *120*, 9506−9510.

(16) Qian, X.; Liu, J.; Fu, L.; Li, J. Quantum Spin Hall Effect in Two-Dimensional Transition Metal Dichalcogenides. *Science* **2014**, *346*, 1344−1347.

(17) Johari, P.; Shenoy, V. B. Tunable Dielectric Properties of Transition Metal Dichalcogenides. *ACS Nano* **2011**, *5*, 5903−5908.

(18) Mak, K. F.; He, K.; Shan, J.; Heinz, T. F. Control of Valley Polarization in Monolayer MoS_2 by Optical Helicity. *Nat. Nanotechnol.* **2012**, *7*, 494−498.

(19) Roy, K.; Padmanabhan, M.; Goswami, S.; Sai, T. P.; Ramalingam, G.; Raghavan, S.; Ghosh, A. Graphene-MoS_2 Hybrid Structures for Multifunctional Photoresponsive Memory Devices. *Nat. Nanotechnol.* **2013**, *8*, 826−830.

(20) Gong, C.; Colombo, L.; Wallace, R. M.; Cho, K. The Unusual Mechanism of Partial Fermi Level Pinning at Metal-MoS_2 Interfaces. *Nano Lett.* **2014**, *14*, 1714−1720.

(21) Liu, W.; Kang, J.; Sarkar, D.; Khatami, Y.; Jena, D.; Banerjee, K. Role of Metal Contacts in Designing High-Performance Monolayer n-type WSe_2 Field Effect Transistors. *Nano Lett.* **2013**, *13*, 1983−1990.

(22) Fang, H.; Chuang, S.; Chang, T. C.; Takei, K.; Takahashi, T.; Javey, A. High-Performance Single Layered WSe_2 p-FETs with Chemically Doped Contacts. *Nano Lett.* **2012**, *12*, 3788−3792.

(23) Schmidt, H.; Giustiniano, F.; Eda, G. Electronic Transport Properties of Transition Metal Dichalcogenide Field-Effect Devices: Surface and Interface Effects. *Chem. Soc. Rev.* **2015**, *44*, 7715−7736.

(24) Fang, H.; Tosun, M.; Seol, G.; Chang, T. C.; Takei, K.; Guo, J.; Javey, A. Degenerate n-Doping of Few-Layer Transition Metal Dichalcogenides by Potassium. *Nano Lett.* **2013**, *13*, 1991−1995.

(25) Kang, D.−H.; Shim, J.; Jang, S. K.; Jeon, J.; Jeon, M. H.; Yeom, G. Y.; Jung, W.−S.; Jang, Y. H.; Lee, S.; Park, J.−H. Controllable Nondegenerate p-type Doping of Tungsten Diselenide by Octadecyltrichlorosilane. *ACS Nano* **2015**, *9*, 1099−1107.

(26) Chen, M.; Nam, H.; Wi, S.; Ji, L.; Ren, X.; Bian, L.; Lu, S.; Liang, X. Stable Few-Layer MoS_2 Rectifying Diodes Formed by Plasma-Assisted Doping. *Appl. Phys. Lett.* **2013**, *103*, 142110.

(27) Xi, J.; Zhao, T.; Wang, D.; Shuai, Z. Tunable Electronic Propereties of Two-Dimensional Transition Metal Dichalcogenide Alloys: A First-Principles Prediction. *J. Phys. Chem. Lett.* **2014**, *5*, 285−291.

(28) Huang, L.; Li, B.; Zhong, M.; Wei, Z.; Li, J. Tunable Schottky Barrier at MoSe2/Metal Interfaces with a Buffer Layer. *J. Phys. Chem. C* **2017**, *121*, 9305−9311.

(29) Wi, S.; Chen, M.; Li, D.; Nam, H.; Meyhofer, E.; Liang, X. Photovoltaic Response in Pristine WSe_2 Layers Modulated by Metal-Induced Surface-Charge-Transfer Doping. *Appl. Phys. Lett.* **2015**, *107*, 062102.

(30) Chen, C.−H.; Wu, C.−L.; Pu, J.; Chiu, M. − H.; Kumar, P.; Takenobu, T.; Li, L.−J. Hole Mobility Enhancement and p-Doping in Monolayer WSe_2 by Gold Decoration. *2D Mater.* **2014**, *1*, 034001.

(31) Podzorov, V.; Gershenson, M. E.; Kloc, Ch.; Zeis, R.; Bucher, E. High-Mobility Field-Effect Transistors Based on Transition Metal Dichalcogenides. *Appl. Phys. Lett.* **2004**, *84*, 3301−3303.

(32) Nourbakhsh, A.; Zubair, A.; Sajjad, R. N.; Tavakkoli K. G., A.; Chen, W.; Fang, S.; Ling, X.; Kong, J.; Dresselhaus, M. S.; Kaxiras, E.; et al. MoS_2 Field-Effect Transistor with Sub-10 nm Channel Length. *Nano Lett.* **2016**, *16*, 7798−7806.

(33) Hsieh, K.; Kochat, V.; Zhang, X.; Gong, Y.; Tiwary, C. S.; Ajayan, P. M.; Ghosh, A. Effect of Carrier Localization on Electrical Transport and Noise at Individual Grain Boundaries in Monolayer MoS_2. *Nano Lett.* **2017**, *17*, 5452−5457.

(34) Nakaharai, S.; Yamamoto, M.; Ueno, K.; Lin, Y.-F.; Li, S.-L.; Tsukagoshi, K. Electrostatically Reversible Polarity of Ambipolar α-$MoTe_2$ Transistors. *ACS Nano* **2015**, *9*, 5976−5983.

(35) Baugher, B. W. H.; Churchill, H. O. H.; Yang, Y.; Jarillo-Herrero, P. Optoelectronic Devices Based on Electrically Tunable p-n Diodes in a Monolayer Dichalcogenide. *Nat. Nanotechnol.* **2014**, *9*, 262−267.

(36) Lopez-Sanchez, O.; Lembke, D.; Kayci, M.; Radenovic, A.; Kis, A. Ultrasensitive Photodetectors Based on Monolayer MoS_2. *Nat. Nanotechnol.* **2013**, *8*, 497−501.

DOI: 10.1021/acs.jpcc.8b05857
J. Phys. Chem. C 2018, 122, 17001−17007

(37) Yang, Y.; Fang, W.-H.; Long, R. Disparity in Photoexcitation Dynamics Between Vertical and Lateral MoS_2/WSe_2 Heterojunctions: Time-Domain Simulation Emphasizes the Importance of Donor-Acceptor Interaction and Band Alignment. *J. Phys. Chem. Lett.* **2017**, *8*, 5771−5778.

(38) Li, Y.; Rao, Y.; Mak, K. F.; You, Y.; Wang, S.; Dean, C. R.; Heinz, T. F. Probing Symmetry Properties of Few-Layer MoS_2 and h-BN by Optical Second-Harmonic Generation. *Nano Lett.* **2013**, *13*, 3329−3333.

(39) Ahmad, R.; Srivastava, R.; Yadav, S.; Singh, D.; Gupta, G.; Chand, S.; Sapra, S. Functionalized Molybdenum Disulfide Nanosheets for 0D − 2D Hybrid Nanostructures: Photoinduced Charge Transfer and Enhanced Photoresponse. *J. Phys. Chem. Lett.* **2017**, *8*, 1729−1738.

(40) Radisavljevic, B.; Radenovic, A.; Brivio, J.; Giacometti, V.; Kis, A. Single-layer MoS_2 transistors. *Nat. Nanotechnol.* **2011**, *6*, 147−150.

(41) Yamamoto, M.; Einstein, T. L.; Fuhrer, M. S.; Cullen, W. G. Anisotropic Etching of Atomically Thin MoS_2. *J. Phys. Chem. C* **2013**, *117*, 25643−25649.

(42) Yamamoto, M.; Dutta, S.; Aikawa, S.; Nakaharai, S.; Wakabayashi, K.; Fuhrer, M. S.; Ueno, K.; Tsukagoshi, K. Self-Limiting Layer-by-Layer Oxidation of Atomically Thin WSe_2. *Nano Lett.* **2015**, *15*, 2067−2073.

(43) Yamamoto, M.; Nakaharai, S.; Ueno, K.; Tsukagoshi, K. Self-Limiting Oxides on WSe_2 as Controlled Surface Acceptors and Low-Resistance Hole Contacts. *Nano Lett.* **2016**, *16*, 2720−2727.

(44) Wang, Y.; Yang, R. X.; Quhe, R.; Zhong, H.; Cong, L.; Ye, M.; Ni, Z.; Song, Z.; Yang, J.; Shi, J.; Li, J.; Lu, J. Does p-type Ohmic Contact Exist in WSe_2-Metal Interfaces ? *Nanoscale* **2016**, *8*, 1179−1191.

(45) Movva, H. C. P.; Rai, A.; Kang, S.; Kim, K.; Fallahazad, B.; Taniguchi, T.; Watanabe, K.; Tutuc, E.; Banerjee, S. K. High-Mobility Holes in Dual-Gated WSe_2 Field-Effect Transistors. *ACS Nano* **2015**, *9*, 10402−10410.

(46) Pradhan, N. R.; Rhodes, D.; Memaran, S.; Poumirol, J. M.; Smirnov, D.; Talapatra, S.; Feng, S.; Perea-Lopez, N.; Elias, A. L.; Terrones, M.; Ajayan, P. M.; Balicas, L. Hall and Field-Effect Mobilities in Few Layered p-WSe_2 Field-Effect Transistors. *Sci. Rep.* **2015**, *5*, 8979.

(47) Shokouh, S. H. H.; Jeon, P. J.; Pezeshki, A.; Choi, K.; Lee, H. S.; Kim, J. S.; Park, E. Y.; Im, S. High-Performance, Air-Stable, Top-Gate, p-Channel WSe_2 Field-Effect Transistor with Fluoropolymer Buffer Layer. *Adv. Funct. Mater.* **2015**, *25*, 7208−7214.

(48) Chuang, H.−J.; Tan, X.; Ghimire, N. J.; Perera, M. M.; Chamlagain, B.; Cheng, M. M.−C.; Yan, J.; Mandrus, D.; Tománek, D.; Zhou, Z. High Mobility WSe_2 p- and n-type Field-Effect Transistors Contacted by Highly Doped Graphene for Low-Resistance Contacts. *Nano Lett.* **2014**, *14*, 3594−3601.

(49) Soler, J. M.; Artacho, E.; Gale, J. D.; García, A.; Junquera, J.; Ordejón, P.; Sánchez-Portal, D. The SIESTA Method for Ab-initio Order-N Materials Simulation. *J. Phys.: Condens. Matter* **2002**, *14*, 2745−2779.

(50) Perdew, J. P.; Burke, K.; Ernzerhof, M. Generalized Gradient Approximation Made Simple. *Phys. Rev. Lett.* **1996**, *77*, 3865−3868.

(51) Mak, K. F.; Lee, C.; Hone, J.; Shan, J.; Heinz, T. F. Atomically Thin MoS_2: A New Direct-Gap Semiconductor. *Phys. Rev. Lett.* **2010**, *105*, 136805.

(52) Splendiani, A.; Sun, L.; Zhang, Y.; Li, T.; Kim, J.; Chim, C.-Y.; Galli, G.; Wang, F. Emerging Photoluminescence in Monolayer MoS_2. *Nano Lett.* **2010**, *10*, 1271−1275.

(53) Kumar, A.; Ahluwalia, P. K. Electronic Structure of Transition Metal Dichalcogenides Monolayers 1H-MX_2 (M = Mo, W; X = S, Se, Te) from Ab-initio Theory: New Direct Band Gap Semiconductors. *Eur. Phys. J. B* **2012**, *85*, 186.

(54) Irfan; Ding, H.; Gao, Y.; Small, C.; Kim, D. Y.; Subbiah, J.; So, F. Energy Level Evolution of Air and Oxygen Exposed Molybdenum Trioxide Films. *Appl. Phys. Lett.* **2010**, *96*, 243307.

(55) Meyer, J.; Shu, A.; Kröger, M.; Kahn, A. Effect of Contamination on the Electronic Structure and Hole-Injection Properties of MoO_3/Organic Semiconductor Interfaces. *Appl. Phys. Lett.* **2010**, *96*, 133308.

(56) Gwinner, M. C.; Di Pietro, R.; Vaynzof, Y.; Greenberg, K. J.; Ho, P. K. H.; Friend, R. H.; Sirringhaus, H. Doping of Organic Semiconductors using Molybdenum Trioxide: A Quantitative Time-Dependent Electrical and Spectroscopic Study. *Adv. Funct. Mater.* **2011**, *21*, 1432−1441.

(57) Battaglia, C.; Yin, X.; Zheng, M.; Sharp, I. D.; Chen, T.; McDonnell, S.; Azcatl, A.; Carraro, C.; Ma, B.; Maboudian, R.; Wallace, R. M.; Javey, A. Hole Selective MoO_x Contact for Silicon Solar Cells. *Nano Lett.* **2014**, *14*, 967−971.

(58) Zhang, Z.; Wei, H.−X.; Ma, G.−F.; Li, Y.−Q.; Lee, S.−T.; Tang, J.−X. Interface Energetics at WO_x/Organic Interfaces: The Role of Oxygen Vacancies. *Appl. Phys. Lett.* **2013**, *103*, 133302.

(59) Zhou, J.; Jena, P. Giant Valley Splitting and Valley Polarized Plasmonics in Group V Transition-Metal Dichalcogenide Monolayers. *J. Phys. Chem. Lett.* **2017**, *8*, 5764−5770.

(60) Movva, H. C. P.; Lovorn, T.; Fallahazad, B.; Larentis, S.; Kim, K.; Taniguchi, T.; Watanabe, K.; Banerjee, S. K.; MacDonald, A. H.; Tutuc, E. Tunable Γ - K Valley Populations in Hole-Doped Trilayer WSe_2. *Phys. Rev. Lett.* **2018**, *120*, 107703.

DOI: 10.1021/acs.jpcc.8b05857
J. Phys. Chem. C 2018, 122, 17001−17007